

Dzyaloshinskii-Moriya interaction and field-free sub-10 nm topological magnetism in Fe/bismuth oxychalcogenides heterostructures

Yaoyuan Wang(王垚元), Long You(游龙), Kai Chang(常凯), and Hongxin Yang(杨洪新)

Citation: Chin. Phys. B, 2024, 33 (**9**): 097508. DOI: 10.1088/1674-1056/ad6a0e
Journal homepage: http://cpb.iphy.ac.cn; http://iopscience.iop.org/cpb

What follows is a list of articles you may be interested in

Interacting topological magnons in a checkerboard ferromagnet

Heng Zhu(朱恒), Hongchao Shi(施洪潮), Zhengguo Tang(唐政国), and Bing Tang(唐炳)
Chin. Phys. B, 2024, 33 (**3**): 037503. DOI: 10.1088/1674-1056/ad01a2

Oscillation of Dzyaloshinskii-Moriya interaction driven by weak electric fields

Runze Chen(陈润泽), Anni Cao(曹安妮), Xinran Wang(王馨苒), Yang Liu(柳洋), Hongxin Yang(杨洪新), and Weisheng Zhao(赵巍胜)
Chin. Phys. B, 2024, 33 (**2**): 027501. DOI: 10.1088/1674-1056/ad0f85

Influence of Dzyaloshinskii-Moriya interaction on the magnetic vortex reversal in an off-centered nanocontact geometry

Hua-Nan Li(李化南), Tong-Xin Xue(薛彤鑫), Lei Chen(陈磊), Ying-Rui Sui(隋瑛瑞), and Mao-Bin Wei(魏茂彬)†
Chin. Phys. B, 2022, 31 (**9**): 097501. DOI: 10.1088/1674-1056/ac4cbd

Synchronization of nanowire-based spin Hall nano-oscillators

Biao Jiang(姜彪), Wen-Jun Zhang(张文君), Mehran Khan Alam, Shu-Yun Yu(于淑云), Guang-Bing Han(韩广兵), Guo-Lei Liu(刘国磊), Shi-Shen Yan(颜世申), and Shi-Shou Kang(康仕寿)
Chin. Phys. B, 2022, 31 (**7**): 077503. DOI: 10.1088/1674-1056/ac560a

Exact soliton solutions in anisotropic ferromagnetic wires with Dzyaloshinskii-Moriya interaction

Qiu-Yan Li(李秋艳), Dun-Zhao(赵敦), and Zai-Dong Li(李再东)
Chin. Phys. B, 2021, 30 (**1**): 017504. DOI: 10.1088/1674-1056/abca26

RAPID COMMUNICATION

Dzyaloshinskii–Moriya interaction and field-free sub-10 nm topological magnetism in Fe/bismuth oxychalcogenides heterostructures

Yaoyuan Wang(王垚元)[1,2], Long You(游龙)[1,3,†], Kai Chang(常凯)[2], and Hongxin Yang(杨洪新)[2,‡]

[1] *School of Integrated Circuits, Huazhong University of Science and Technology, Wuhan* 430074, *China*
[2] *Center for Quantum Matter, School of Physics, Zhejiang University, Hangzhou* 310058, *China*
[3] *Shenzhen Huazhong University of Science and Technology Research Institute, Shenzhen* 518000, *China*

(Received 9 July 2024; revised manuscript received 30 July 2024; accepted manuscript online 1 August 2024)

Topological magnetism with strong robustness, nanoscale dimensions and ultralow driving current density ($\sim 10^6$ A/m^2) is promising for applications in information sensing, storage, and processing, and thus sparking widespread research interest. Exploring candidate material systems with nanoscale size and easily tunable properties is a key for realizing practical topological magnetism-based spintronic devices. Here, we propose a class of ultrathin heterostructures, Fe/Bi_2O_2X (X = S, Se, Te) by deposing metal Fe on quasi-two-dimensional (2D) bismuth oxychalcogenides Bi_2O_2X (X = S, Se, Te) with excellent ferroelectric/ferroelastic properties. Large Dzyaloshinskii–Moriya interaction (DMI) and topological magnetism can be realized. Our atomistic spin dynamics simulations demonstrate that field-free vortex–antivortex loops and sub-10 nm skyrmions exist in Fe/Bi_2O_2S and Fe/Bi_2O_2Se interfaces, respectively. These results provide a possible strategy to tailor topological magnetism in ultrathin magnets/2D materials interfaces, which is extremely vital for spintronics applications.

Keywords: Dzyaloshinskii–Moriya interaction, field-free, topological magnetism

PACS: 75.30.–m, 75.78.Cd, 12.39.Dc, 67.80.dk **DOI:** 10.1088/1674-1056/ad6a0e

Dzyaloshinskii–Moriya interaction (DMI)[1,2] is an antisymmetric exchange coupling interaction that occurs in systems with broken inversion symmetry[3] and spin–orbit coupling (SOC). Unlike the Heisenberg exchange coupling which aligns spins in a collinear manner, DMI drives spins to be noncollinear mutually. DMI plays a crucial role in the formation of topological magnetism, such as skyrmions,[4,5] bimerons[6] and chiral domain walls (DWs).[7,8] And DMI can also induce topologically nontrivial magnon excitations.[9,10] The topological magnetic structures possess rich properties like topological protection, topological Hall effect,[11,12] ultra-low driving current density ($\sim 10^6$ A/m^2)[13–15] and have broad application prospects in spintronic devices, thus arousing extensive research interest. Especially, skyrmions can serve as information carriers in racetrack memories,[16] spintronic logic devices,[17–19] as well as artificial synapses used in neuromorphic computing.[20] At present, skyrmions and chiral domain walls have been successfully demonstrated experimentally for memory applications.[21,22] Many researches have clarified that DMI can be induced at the ferromagnet (FM)/oxide[23] and FM/ferroelectric (FE)[24,25] interfaces, in heavy metal (HM)/FM multilayers,[26] 2D Janus magnets,[27–31] intrinsic multiferroics,[32–35] curvature-induced 2D structures[36–38] and Morié pattern.[39,40] Enhancing DMI intensity is critical for the generation and stabilization of topological magnetism.[41] Strategies to achieve this include altering the thickness of FM[28,42] or HM[26,43] layers, employing strain engineering,[44–46] or applying an external electric field.[47] At present, exploring more novel material systems capable of achieving large DMI is still urgent for developing skyrmions-based ultralow-power spintronic devices.

Bi_2O_2X (X = S, Se, Te) are a family of layered quasi-2D materials and structurally formed by alternating stacking of positively charged $[Bi_2O_2]^{2+}$ layers and negatively charged X^{2-} layers. Due to the weak interlayer interactions, they are easier to miniaturize and regulate compared to bulk materials. And they possess excellent ferroelectric/ferroelastic properties, strong SOC and high electron mobility,[48–55] of which the polarization states can be switched by applying strain[55] or electric field.[56] Therein, Bi_2O_2Se exhibits room-temperature ferroelectricity and can maintain the ferroelectric order in 2 nm ultrathin film.[50] However, there is no intrinsic DMI due to the absence of magnetism in Bi_2O_2X. There is an extremely lack of research on Bi_2O_2X-based heterostructures currently. As mentioned above, DMI has been observed in many FM/FE systems, such as Co/VSe_2,[57] Co/$PbTiO_3$[58] and Fe_3GeTe_2/In_2Se_3.[24] This type of metal/ferroic heterostructure can be fabricated in experiment, like the prepa-

†Corresponding author. E-mail: lyou@hust.edu.cn
‡Corresponding author. E-mail: hongxin.yang@zju.edu.cn

© 2024 Chinese Physical Society and IOP Publishing Ltd

ration of Co/VSe_2 in Ref. [57]. Due to the ultrathin metal layer, the applied external electric field can penetrate the interface and act on the FE substrate.[59] Furthermore, the power consumption of FM/FE stacks is limited due to the low ferroelectric reverse voltage, which can be used in low-power spintronic devices.

In this paper, we clarify that the DMI and topological quasiparticles can be realized in Fe/Bi_2O_2X ultrathin heterostructures. The magnetic properties of their undistorted and distorted states are studied and large DMI originating from the interfacial heavy Bi element is discovered in Fe/Bi_2O_2S(Se) systems which decreases with an increase in the number of Fe atomic layers. Our atomistic spin dynamics simulations demonstrate that the zero-field spin textures of vortex–antivortex loops and sub-10 nm skyrmions are realized in Fe/Bi_2O_2S(Se). These topological quasiparticles closely related to DMI can be modulated by structural distortions caused by strain engineering due to the inherent FE/ferroelastic effect of the Bi_2O_2X substrate.

We perform the first-principles calculations by using the Vienna *Ab initio* Simulation Package (VASP)[60–62] within the framework of density functional theory (DFT). The generalized gradient approximation (GGA)[63] of Perdew–Burke–Ernzerhof (PBE) forms is used to describe the exchange–correlation effect. And to handle the interaction between core electrons and valence electrons, the projector augmented plane wave (PAW) method[64] is employed. We set the cutoff energy of the plane wave basis to 450 eV and use a Γ-centered $12\times12\times1$ k-point grid in the Brillouin zone for heterostructural optimization. Meanwhile, the DFT-D3 scheme[65] is taken into account to simulate van der Waals interactions. The bottom-site X atoms are passivated with hydrogen atoms to balance the non-stoichiometry.[66,67] All the structures are fully relaxed until the Hellmann–Feynman force on each atom becomes less than 0.001 eV/Å and the convergence criterion for the total energy of ion relaxation process is less than 1×10^{-7} eV. Besides, we adopt a Γ-centered $20\times20\times1$ k-point grid for the calculation of Heisenberg exchange coupling and magnetic anisotropy, and an $8\times16\times1$ k-point mesh for $2\sqrt{2}\times\sqrt{2}\times1$ supercell in the calculation of DMI [see supplemental materials (SM) for details].

Figure 1(a) is the schematic diagram of the atomic structure of the heterostructure we study, which is composed of one layer of Fe atoms and two layers of Bi_2O_2X (X = S, Se, Te). The thickness of vacuum zone is set to be larger than 15 Å along z direction to avoid the interaction of periodic images. We have tested different stacking configurations of the heterostructures as shown in Figs. S1(a) and S1(b), where the most stable configuration displays that the interfacial Fe atoms prefer to be in the middle of the nearest-neighbor (NN) X atoms in the top view. The structure seen in Fig. 1(a) is undistorted, where the atoms are located at equilibrium positions and the space group is I_4/mmm. And Fe/Bi_2O_2X (X = S, Se, Te) also have distorted states in different cases as demonstrated in Fig. S2. All heterostructures release energy during their formation, indicating their thermodynamic stability (see Fig. S3). It is worth noting that for Fe/Bi_2O_2S and Fe/Bi_2O_2Se, two distorted structures are equivalent. For Fe/Bi_2O_2S(Se), the distorted-II structure is equivalent to rotating the distorted-I structure around the z-axis by 90° (180°). Therefore, in the following text, we only focus on the distorted-I structure of them. We fix the in-plane lattice constants of the undistorted heterostructures as $a=b=3.849$ Å for Fe/Bi_2O_2S; $a=b=$ 3.906 Å for Fe/Bi_2O_2Se; $a=b=4.010$ Å for Fe/Bi_2O_2Te, which are well consistent with Ref. [49]. The structural transformation between the undistorted states and the distorted states can be accomplished by applying a strain, which is discussed in SM. The presence of Fe atoms at the interface breaks the inversion symmetry of the systems, which is necessary for harboring DM interaction.

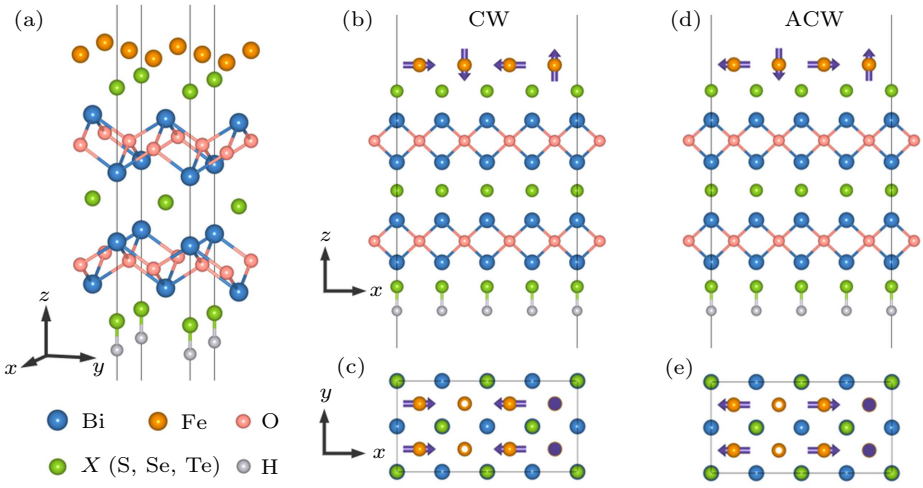


Fig. 1. (a) The atomic structure of Fe/Bi_2O_2X (X = S, Se, Te) ultrathin heterostructure. (b), (c) Clockwise and (d), (e) anti-clockwise spin configurations of $2\sqrt{2}\times\sqrt{2}\times1$ supercell used to calculate the DMI.

Upon all these undistorted and distorted states, we systematically study the magnetic parameters, including Heisenberg exchange coupling, magnetic anisotropy energy (MAE) and DMI through first-principles calculations. We bring in the following spin Hamiltonian:

$$H = -J\sum_{\langle i,j\rangle} \boldsymbol{S}_i \cdot \boldsymbol{S}_j - K\sum_i (S_i^z)^2 - \sum_{\langle i,j\rangle} \boldsymbol{d}_{ij} \cdot (\boldsymbol{S}_i \times \boldsymbol{S}_j), \quad (1)$$

in which $\boldsymbol{S}_i$ is the unit spin vector of Fe atom at site i, J represents the NN exchange coupling constant, K indicates the magnetic anisotropy constant, and $\boldsymbol{d}_{ij}$ means DMI between the NN Fe atom pairs.

Based on the relaxed structures, we adopt the spin-spiral calculations in real space[26,68] to obtain the DMI strength, d_{tot}. Figures 1(b), 1(c) and 1(d), 1(e) respectively show clockwise (CW) and anti-clockwise (ACW) spin configurations of $2\sqrt{2}\times\sqrt{2}\times 1$ supercell. By comparing the energy difference of CW and ACW chiral spin configurations, we get the DMI value $d_{\text{tot}} = (E_{\text{CW}} - E_{\text{ACW}})/16$. All the detailed derivations of J, K and d_{tot} can be found in SM. We demonstrate that the Heisenberg exchange coupling of Fe/Bi_2O_2X is isotropic (see Table S3). The histograms of calculated J, K, and d_{tot} changing with structures are exhibited in Fig. 2, and the specific values are listed in Table S1. Here $J > 0/J < 0$ denotes the FM/ antiferromagnetic coupling; $K > 0/K < 0$ represents the perpendicular/in-plane magnetic anisotropy (PMA/IMA); $d_{\text{tot}} < 0$ ($d_{\text{tot}} > 0$) indicates the CW (ACW) chirality.

It can be seen in Fig. 2(a) that all the stacks are FM coupling, and the Heisenberg exchange coupling interactions are strong (> 30 meV). The distortions can't change the sign of J and the J values are further increased under distorted conditions. Now we focus on the varieties of MAE and DMI in Figs. 2(b) and 2(c). In Fe/Bi_2O_2S and Fe/Bi_2O_2Se stacks, distortions reduce their DMI strength and change them from IMA to PMA. And for Fe/Bi_2O_2Te, distortion-I enhances its DMI strength and transforms it from IMA to PMA, while distortion-II has almost no effect due to its negligible structural differences. In spite of this, the DMI value of Fe/Bi_2O_2Te is still smaller than others. We have analyzed the atomic-layer-resolved SOC energy related to MAE, $\Delta E_{\text{SOC}}^{\text{MAE}}$, in all stacks to identify the reasons for such changes in MAE (see Figs. S8 and S9). For undistorted Fe/Bi_2O_2X (X = S, Se, Te) in Figs. S8(a), S8(b) and S9(a), atoms Bi_1 near the interface make significant contributions, while the interfacial Fe and X elements produce collaborative contributions, leading to the IMA. In detail, the interfacial S/Se atom almost has no contribution while the interfacial Te atom contributes a lot, and Bi_1 contributes more in Fe/Bi_2O_2Se(Te) systems than in Fe/Bi_2O_2S. So the MAE amplitude of undistorted Fe/Bi_2O_2Se(Te) is larger. However, for distorted cases in Figs. S8(c), S8(d) and S9(b), element Fe makes reverse contribution and the contribution of atom Bi_1 becomes smaller or even opposite, while that of atom Bi_2 is enhanced, causing their transition from IMA to PMA.

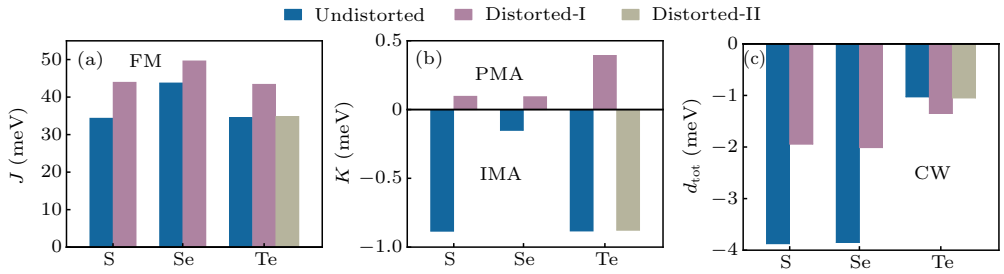


Fig. 2. Calculated (a) the nearest neighbor exchange coupling constants J, (b) magnetic anisotropy constant K, and (c) DMI strength d_{tot} for undistorted and distorted Fe/Bi_2O_2X stacks.

To explore the origin of DMI, the schematic diagram of atomic-layer-resolved SOC energy associated with the DMI of Fe/Bi_2O_2X, $\Delta E_{\text{SOC}}^{\text{DMI}}$, is plotted through comparing the SOC energy of the opposite chiral spin configurations. Figure 3 shows the extracted $\Delta E_{\text{SOC}}^{\text{DMI}}$ of Fe/Bi_2O_2S(Se), and the DMI mainly originates from the heavy metal atom Bi_1 relatively close to the interface, rather than the atom S_1/Se_1 that is the closest to the interface, which conforms to the Fert–Lévy mechanism of DMI.[3,16] In undistorted Fe/Bi_2O_2S(Se), the contribution of S_1/Se_1 is opposite to that of Bi_1, and the SOC contribution generated by S_1 is smaller and almost negligible compared with Se_1, so the DMI of Fe/Bi_2O_2S is a little stronger than that of Fe/Bi_2O_2Se. When the structure is distorted, even if the contribution from atom S_1/Se_1 is reversed, the most important contribution from Bi_1 becomes too small, resulting in a weaker DMI. Furthermore, the contributions of S_1 and Bi_1 in distorted Fe/Bi_2O_2S are smaller than those of Se_1 and Bi_1 in distorted Fe/Bi_2O_2Se, resulting in a slightly stronger DMI of the latter. However, for Fe/Bi_2O_2Te (see Fig. S10), the competing contribution generated by the interfacial heavy atom Te_1 increases greatly and even exceeds that of heavy atom Bi_1, leading to the overall DMI decreasing. In its distorted-I structure, the beneficial contribution from element Fe is significantly enhanced, while the competing contribution from atom Te_1 is weakened, so the DMI strength increases. The distribution of SOC contributions in the distorted-II structure only differs slightly from the undistorted case, arising from the minor difference in their structures.

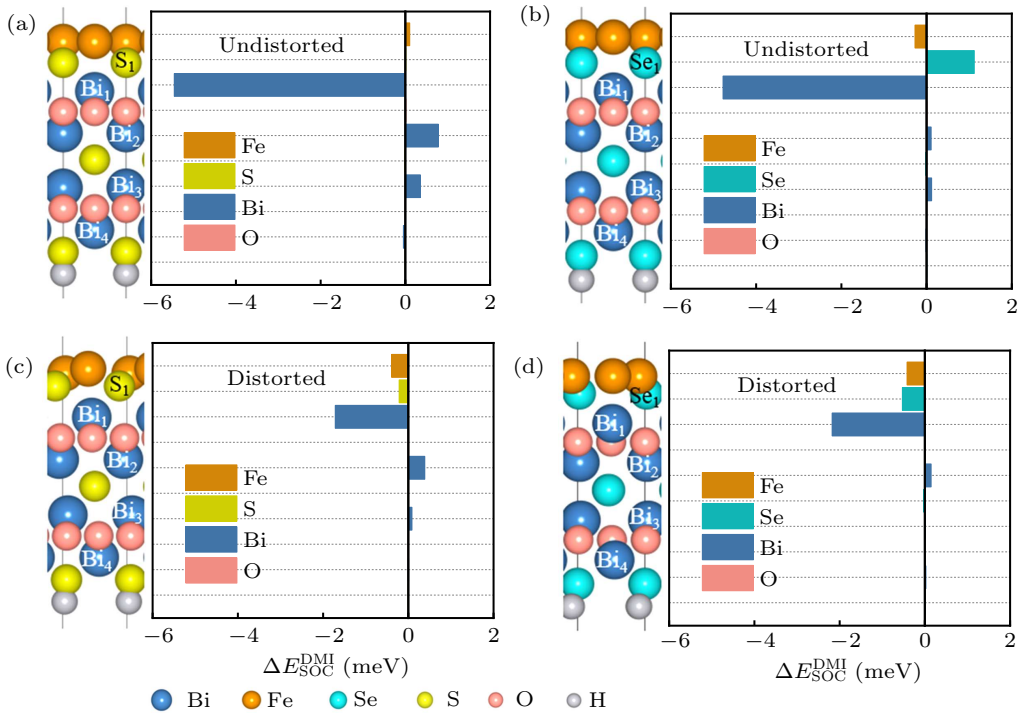


Fig. 3. Atomic-layer-resolved SOC energy associated with DMI of (a) undistorted, (c) distorted Bi_2O_2S/Fe and (b) undistorted, (d) distorted Bi_2O_2Se/Fe.

Significantly, there are quite sizable DMI amplitudes of 3.872 (3.850) meV/atom in undistorted Fe/Bi_2O_2S(Se) stacks, stronger than the DMI in traditional systems, like Co/Pt bilayer (3.05 meV/atom),[41,69] Janus MnSTe (2.86 meV/atom)[28] and Fe/Ir(111) (1.7 meV/atom).[70] Such large DMI amplitudes also result in the large $|d_{tot}/J|$, 0.113 (0.088) for undistorted Fe/Bi_2O_2S(Se), which are quite close to the typical range of 0.10–0.20 for the topological magnetic structures formation.[16] However, the topological magnetic structures are synergistically determined by d_{tot}, K, and J. d_{tot} favors the generation of non-collinear spin spirals, but J and K tend to align the spins collinearly. The effect of MAE is ignored when evaluating spin textures using $|d_{tot}/J|$, which may cause deviation. So, we introduce another dimensionless parameter $\kappa = \left|\left(\frac{4}{\pi}\right)^2 \frac{2JK}{d_{tot}^2}\right|$[71] to jointly evaluate the generation of spin textures, which is listed in Table S1. The calculated κ of the Fe/Bi_2O_2S(Se) is moderate ($1 < \kappa < 7$) with $|d_{tot}/J|$ greater than 0.04, which may lead to the generation of isolated skyrmions, but the κ of the Fe/Bi_2O_2Te may be too large (> 30) to generate them.[71–73] In addition, the large values of J and d_{tot} are beneficial for preventing the annihilation of topological magnetism.[74]

After the magnetic parameters J, K, and d_{tot} of spin Hamiltonian H are obtained, the formations of spin textures are verified by carrying out atomistic spin dynamics simulations with the SPIRIT software package.[75] The spin dynamic evolution process can be described by the Landau–Lifshitz–Gilbert (LLG) equation:

$$\frac{\partial \boldsymbol{S}_i}{\partial t} = -\frac{\gamma}{1+\alpha^2}[\boldsymbol{S}_i \times \boldsymbol{B}_{\text{eff}}^i + \alpha \boldsymbol{S}_i \times (\boldsymbol{S}_i \times \boldsymbol{B}_{\text{eff}}^i)], \quad (2)$$

in which γ is the gyromagnetic ratio, α indicates the damping constant and is set to 0.2, and $\boldsymbol{B}_{\text{eff}}^i$ represents the effective field of site i,

$$\boldsymbol{B}_{\text{eff}}^i = -\frac{1}{\mu_S}\frac{\partial H}{\partial \boldsymbol{S}_i}. \quad (3)$$

A 40 nm×40 nm supercell with 150×150 atoms under in-plane periodic boundary conditions is constructed to obtain complete spin textures. In the simulations, at the temperature of 0 K, random magnetic states are used as the initial states and the number of iteration steps is set to 2×10^5 to acquire the stable ground states without applying external magnetic field. In undistorted Fe/Bi_2O_2S system, vortex–antivortex loops (VALs) appear [see Fig. 4(a)], arising from the relatively giant values of the CW chiral DMI (3.872 meV/atom) and IMA (1.768 meV/f.u.).[37,76,77] And there are Néel-type skyrmions (Sk) with the diameters of 8 nm–10 nm as well as skyrmionium [see Fig. 4(c)] in undistorted Fe/Bi_2O_2Se system, attributing to the similar DMI (3.850 meV/atom) and even smaller IMA (0.302 meV/f.u.) compared to those of Fe/Bi_2O_2S. Once the structures are distorted, the VALs in Fe/Bi_2O_2S are changed to skyrmions with the diameter of 6 nm and large size magnetic domains with Néel-type DWs [see Fig. 4(b)]. Meanwhile, the complex case in Fe/Bi_2O_2Se becomes a simple skyrmion lattice with a larger diameter of 14 nm [see Fig. 4(d)]. These are attributed to the reduction of DMI, the out-of-plane transformation of magnetic anisotropy and the enhancement of exchange coupling. However, because of the weak DMI and strong FM exchange coupling, only uniform FM single domain (see Fig. S11) is obtained in Fe/Bi_2O_2Te system, consistent with its large κ. We also

test the effect of the next-nearest neighbor (NNN) exchange coupling on topological spin textures, as shown in Fig. S6. The results indicate that the fundamental magnetic phases of Fe/Bi_2O_2S(Se) remain unchanged.

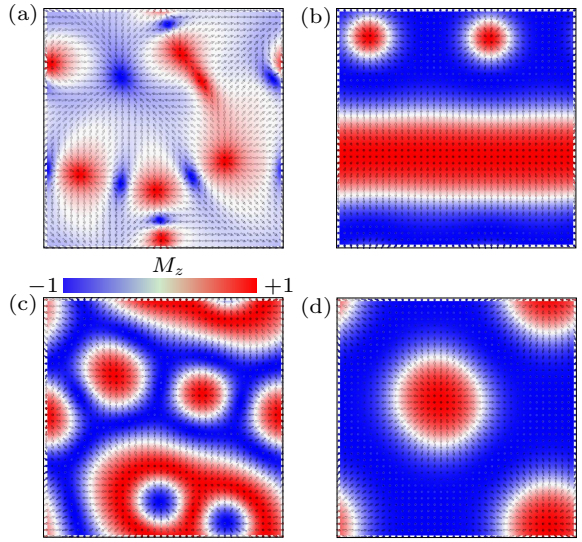


Fig. 4. The relaxed atomistic spin dynamics simulations of (a) undistorted, (b) distorted Bi_2O_2S/Fe and (c) undistorted, (d) distorted Bi_2O_2Se/Fe in real space without applying external magnetic field.

Notably, under the influence of such an IMA (0.302 meV/f.u.) in undistorted Fe/Bi_2O_2Se, the skyrmions emerge [see Fig. 4(c)], which are typically produced under the background of collinear out-of-plane magnetic ordering.[25,77,78] In order to explore the reasons for this situation, we separately test the effects of d_{tot} and J on its spin textures while keeping everything else constant, as shown in Fig. 5. One can see that J mainly influences the size and density of spin spirals, but cannot change their types [see Figs. 5(a)–5(d)]. The initial J equals 43.739 meV in Fig. 4(c), with a corresponding κ value of 1.445, very close to the typical range $0 < \kappa < 1$ for the formation of spin spirals.[34,71] Since κ is directly proportional to J, when J decreases, κ also decreases, dropping to 0.330 in Fig. 5(d), which matches more within the range of 0–1. This leads to the formation of DW and skyrmions, ultimately forming labyrinth domains.[79] In contrast, d_{tot} determines the transition from skyrmions to bimerons [see Figs. 5(e)–5(h)]. Due to the large DMI strength, the in-plane background magnetic order is pulled to the out-of-plane direction, but as the DMI strength decreases, it is restored to the in-plane direction dominated by IMA. In general, the formation of skyrmions in Fig. 4(c) is mainly because of the influence of large DMI. Compared to the large J and d_{tot} values, the IMA is too weak to stabilize the background magnetic order along the in-plane direction.[80] Subsequently, when an in-plane magnetic field is applied to undistorted Fe/Bi_2O_2S along $+x$ direction (B_x), B_x and IMA synergistically transform the VALs into a bimeron chain which is arranged along the direction of magnetic field (see Fig. S12). Especially with large enough B_x (≥ 0.3 T), the chain of bimerons is finally separated into isolated bimerons with a diameter as low as 5 nm in Figs. S12(c) and S12(d).

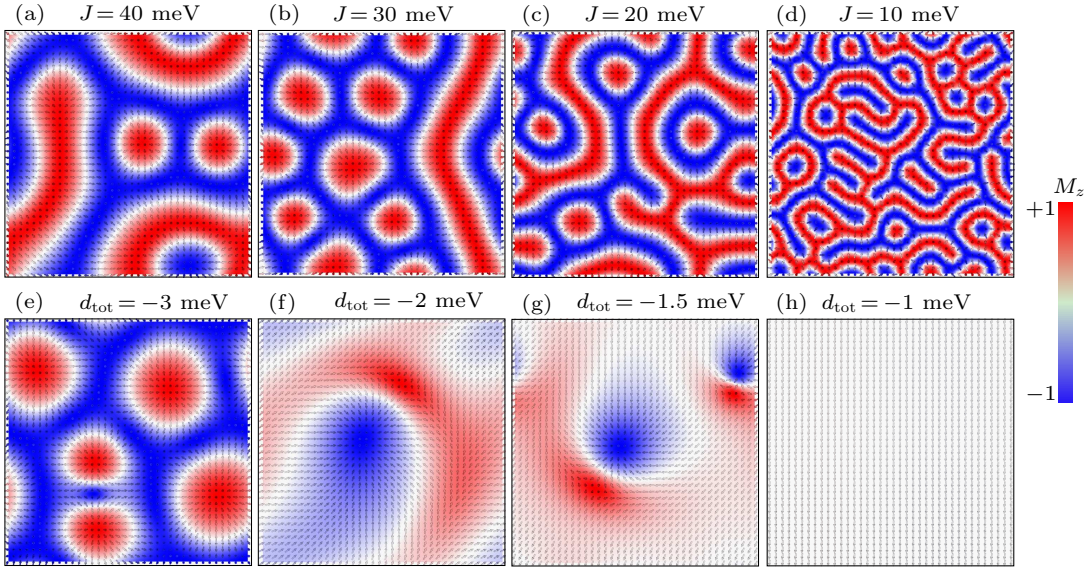


Fig. 5. The evolution of spin textures with (a)–(d) J varying from 40 meV to 10 meV and (e)–(h) d_{tot} varying from −3 meV to −1 meV in undistorted Fe/Bi_2O_2Se.

We summarize some materials that host topological spin textures with sizes smaller than 100 nm based on experimental (Exp.) measurements or theoretical simulations (Sim.) in Table 1. One can see that spin textures found in bulk materials and multilayer films typically exhibit larger sizes of tens of nanometers.[81–84] Additionally, several theoretical studies have successfully induced small-sized (10–23 nm) topological magnetic structures in 2D magnetic thin films.[25,71,85] In comparison, the sub-10 nm VALs and Néel skyrmions that we find in Fe/Bi_2O_2X (X = S, Se) heterostructures are competitive.

Table 1. List of materials hosting skyrmions or other topological spin textures.

Material	Method	Spin texture	Size of spin texture (nm)	Reference
MnSi	Exp.	bloch Sk	18	[81]
Cu_2OSeO_3	Exp.	bloch Sk	62	[83]
$(Ir/Co/Pt)_{10}$	Exp.	Néel Sk	30–90	[84]
$LaCl/In_2Se_3$	Sim.	bimerons	23	[25]
VO_2 monolayer	Sim.	anti-Sk	10	[71]
$CrIn X_3$ (X = Te, Se)	Sim.	Néel Sk	~ 10	[85]
$[Ir/Fe/Co/Pt]_3/W/CoFeB/MgO$	Exp.	Néel Sk	~ 100	[82]
Fe/Bi_2O_2X (X = S, Se)	Sim.	VALs, Néel Sk	~ 10	this paper

On this basis, we further investigate the variation of DMI in undistorted Fe(n ML)/Bi_2O_2S(Se) stacks with the increasing number of Fe monolayers (ML), denoted as n. As shown in Fig. 6, with n varying from 1 to 5, the DMI strength generally tends to decrease. This indicates that this type of DMI is an interfacial effect, the thicker the Fe atomic layers, the weaker the interfacial effect. It is consistent with the change of Co/Pt heterostructure in Ref. [26], in which DMI decreases with the increase of Co atomic layers.

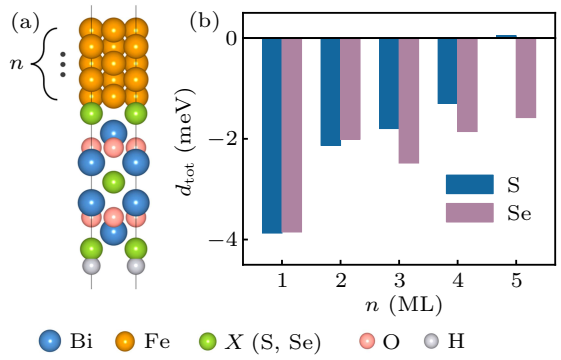


Fig. 6. (a) The side view of Fe (n ML)/Bi_2O_2X (X = S, Se) heterostructure. (b) The total DMI d_{tot} as functions of X and n in (a).

In conclusion, we have explored the DMI and topological magnetic structures in Fe/Bi_2O_2X (X = S, Se, Te) heterostructures. It is shown that the presence of Fe atoms can change the system's symmetry, induce gaint DMI and realize topological magnetic structures without external magnetic field. The distortions caused by strain can effectively modulate the DMI of the heterostructures, and lead to the varieties of VALs or skyrmions. And the DMI is gradually weakened with the increase in the thickness of Fe atoms. Such field-free stabilized sub-10 nm spin textures can be employed for information encoding and storage, while also playing a significant role in advancing the development of next-generation energy-efficient nanoscale spintronic devices based on topological quasi-particles. Therefore, this work enriches the material systems of skyrmions and lays the foundation for the application of skyrmions in spintronics.

Acknowledgements

Project supported by the National Key Research and Development Program of China (Grant Nos. 2022YFA1405100, 2022YFA1403601, 2020AAA0109005, and 2023YFB4502100), the "Pioneer" and "Leading Goose" R&D Program of Zhejiang Province (Grant No. 2022C01053), the National Natural Science Foundation of China (Grant Nos. 12174405, 12204497, 12327806, and 62074063), and Shenzhen Science and Technology Program (Grant No. JCYJ20220818103410022).

References

[1] Dzyaloshinsky I 1958 *J. Phys. Chem. Solids* **4** 241
[2] Moriya T 1960 *Phys. Rev.* **120** 91
[3] Fert A and Lévy P M 1980 *Phys. Rev. Lett.* **44** 1538
[4] Yu X Z, Kanazawa N, Onose Y, Kimoto K, Zhang W Z, Ishiwata S, Matsui Y and Tokura Y 2011 *Nat. Mater.* **10** 106
[5] Fert A, Reyren N and Cros V 2017 *Nat. Rev. Mater.* **2** 17031
[6] Shen L C, Xia J, Zhang X C, Ezawa M, Tretiakov O A, Liu X X, Zhao G P and Zhou Y 2020 *Phys. Rev. Lett.* **124** 037202
[7] Thiaville A, Rohart S, Jué É, Cros V and Fert A 2012 *Europhys. Lett.* **100** 57002
[8] Cui Q R, Liang J H, Zhu Y M, Yao X and Yang H X 2023 *Chin. Phys. Lett.* **40** 037502
[9] Iacocca E and Heinonen O 2017 *Phys. Rev. Appl.* **8** 034015
[10] Li Y M 2023 *Phys. Rev. Res.* **5** 033026
[11] Kanazawa N, Onose Y, Arima T, Okuyama D, Ohoyama K, Wakimoto S, Kakurai K, Ishiwata S and Tokura Y 2011 *Phys. Rev. Lett.* **106** 156603
[12] Li Y F, Kanazawa N, Yu X Z, Tsukazaki A, Kawasaki M, Ichikawa M, Jin X F, Kagawa F and Tokura Y 2013 *Phys. Rev. Lett.* **110** 117202
[13] Jonietz F, Mühlbauer S, Pfleiderer C, Neubauer A, Münzer W, Bauer A, Adams T, Georgii R, Böni P, Duine R A, Everschor K, Garst M and Rosch A 2010 *Science* **330** 1648
[14] Yu X Z, Kanazawa N, Zhang W Z, Nagai T, Hara T, Kimoto K, Matsui Y, Onose Y and Tokura Y 2012 *Nat. Commun.* **3** 988
[15] Nagaosa N and Tokura Y 2013 *Nat. Nanotechnol.* **8** 899
[16] Fert A, Cros V and Sampaio J 2013 *Nat. Nanotechnol.* **8** 152
[17] Luo S J, Song M, Li X, Zhang Y, Hong J, Yang X F, Zou X C, Xu N and You L 2018 *Nano Lett.* **18** 1180
[18] Luo S J and You L 2021 *APL Mater.* **9** 050901
[19] Yu D X, Yang H X, Chshiev M and Fert A 2022 *Natl. Sci. Rev.* **9** nwac021
[20] Song K M, Jeong J S, Pan B, Zhang X C, Xia J, Cha S, Park T E, Kim K, Finizio S, Raabe J, Chang J, Zhou Y, Zhao W S, Kang W, Ju H and Woo S 2020 *Nat. Electron.* **3** 148
[21] Yu G Q, Upadhyaya P, Shao Q M, Wu H, Yin G, Li X, He C L, Jiang W J, Han X F, Amiri P K and Wang K L 2017 *Nano Lett.* **17** 261
[22] Sheng Y, Wang W Y, Deng Y C, Ji Y, Zheng H Z and Wang K Y 2023 *Natl. Sci. Rev.* **10** nwad093
[23] Wang L M, Ga Y L, Cui Q R, Li P, Liang J H, Zhou Y, Wang S G and Yang H X 2023 *Phys. Rev. B* **108** 214404
[24] Huang K, Shao D F and Tsymbal E Y 2022 *Nano Lett.* **22** 3349
[25] Sun W, Wang W X, Li H, Zhang G B, Chen D, Wang J L and Cheng Z X 2020 *Nat. Commun.* **11** 5930
[26] Yang H X, Thiaville A, Rohart S, Fert A and Chshiev M 2015 *Phys. Rev. Lett.* **115** 267210
[27] Liang J H, Wang W W, Du H F, Hallal A, Garcia K, Chshiev M, Fert A and Yang H X 2020 *Phys. Rev. B* **101** 184401

[28] Ga Y L, Yu D X, Wang L M, Li P, Liang J H and Yang H X 2023 *2D Mater.* **10** 035020
[29] Li P, Yu D X, Liang J H, Ga Y L and Yang H X 2023 *Phys. Rev. B* **107** 054408
[30] Cui Q R, Liang J H, Shao Z J, Cui P and Yang H X 2020 *Phys. Rev. B* **102** 094425
[31] Zhu Y M, Cui Q R, Liang J H, Ga Y L and Yang H X 2022 *2D Mater.* **9** 045030
[32] Liang J H, Cui Q R and Yang H X 2020 *Phys. Rev. B* **102** 220409
[33] Xu C S, Chen P, Tan H X, Yang Y R, Xiang H J and Bellaiche L 2020 *Phys. Rev. Lett.* **125** 037203
[34] Wang L M, Ga Y L, Li P, Yu D X, Jiang J W, Liang J H, Wang S G and Yang H X 2023 *Phys. Rev. B* **108** 054440
[35] Ga Y L, Yu D X, Li Y, Jiang J W, Wang L M, Li P, Liang J H, Feng H, Shi Y G and Yang H X 2024 *Phys. Rev. B* **109** L060402
[36] Edström A, Amoroso D, Picozzi S, Barone P and Stengel M 2022 *Phys. Rev. Lett.* **128** 177202
[37] Ga Y L, Cui Q R, Liang J H, Yu D X, Zhu Y M, Wang L M and Yang H X 2022 *Phys. Rev. B* **106** 054426
[38] Jiang J W, Ga Y L, Li P, Cui Q R, Wang L M, Yu D X, Liang J H and Yang H X 2024 *Phys. Rev. B* **109** 014402
[39] Tong Q J, Liu F, Xiao J and Yao W 2018 *Nano Lett.* **18** 7194
[40] Xiao F P, Chen K Q and Tong Q J 2021 *Phys. Rev. Res.* **3** 013027
[41] Yang H X, Boulle O, Cros V, Fert A and Chshiev M 2018 *Sci. Rep.* **8** 12356
[42] Cho J, Kim N H, Lee S, Kim J S, Lavrijsen R, Solignac A, Yin Y X, Han D S, Van Hoof N J J, Swagten H J M, Koopmans B and You C Y 2015 *Nat. Commun.* **6** 7635
[43] Tacchi S, Troncoso R E, Ahlberg M, Gubbiotti G, Madami M, Åkerman J and Landeros P 2017 *Phys. Rev. Lett.* **118** 147201
[44] Gusev N S, Sadovnikov A V, Nikitov S A, Sapozhnikov M V and Udalov O G 2020 *Phys. Rev. Lett.* **124** 157202
[45] Feng C, Meng F, Wang Y D, Jiang J, Mehmood N, Cao Y, Lv X W, Yang F, Wang L, Zhao Y K, Xie S, Hou Z P, Mi W B, Peng Y, Wang K Y, Gao X S, Yu G H and Liu J M 2021 *Adv. Funct. Mater.* **31** 2008715
[46] Zhu Y M, Cui Q R, Liu B, Zhou T J and Yang H X 2023 *Phys. Rev. B* **108** 134438
[47] Dai B Q, Wu D, Razavi S A, Xu S J, He H, Shu Q Y, Jackson M, Mahfouzi F, Huang H S, Pan Q J, Cheng Y, Qu T, Wang T Y, Tai L X, Wong K, Kioussis N and Wang K L 2023 *Sci. Adv.* **9** eade6836
[48] Wu J X, Yuan H T, Meng M M, Chen C, Sun Y, Chen Z Y, Dang W H, Tan C W, Liu Y J, Yin J B, Zhou Y B, Huang S Y, Xu H Q, Cui Y, Hwang H Y, Liu Z F, Chen Y L, Yan B H and Peng H L 2017 *Nat. Nanotechnol.* **12** 530
[49] Wu M H and Zeng X C 2017 *Nano Lett.* **17** 6309
[50] Ghosh T, Samanta M, Vasdev A, Dolui K, Ghatak J, Das T, Sheet G and Biswas K 2019 *Nano Lett.* **19** 5703
[51] Sun Y, Zhang J, Ye S, Song J and Qu J L 2020 *Adv. Funct. Mater.* **30** 2004480
[52] Li T R, Tu T, Sun Y W, Fu H X, Yu J, Xing L, Wang Z A, Wang H M, Jia R D, Wu J X, Tan C W, Liang Y, Zhang Y C, Zhang C C, Dai Y M, Qiu C G, Li M, Huang R, Jiao L Y, Lai K J, Yan B H, Gao P and Peng H L 2020 *Nat. Electron.* **3** 473
[53] Wang F K, Yang S J, Wu J, Hu X Z, Li Y, Li H Q, Liu X T, Luo J H and Zhai T Y 2021 *InfoMat* **3** 1251
[54] Ding X, Li M L, Chen P, Zhao Y, Zhao M, Leng H Q, Wang Y, Ali S, Raziq F, Wu X Q, Xiao H Y, Zu X T, Wang Q Y, Vinu A, Yi J B and Qiao L 2022 *Matter* **5** 4274
[55] Wu M Q, Lou Z F, Dai C M, Wang T, Wang J, Zhu Z Y, Xu Z K, Sun T L, Li W B, Zheng X R and Lin X 2023 *Adv. Mater.* **35** 2300450
[56] Wang W J, Meng Y, Zhang Y X, Zhang Z, Wang W, Lai Z X, Xie P S, Li D J, Chen D, Quan Q, Yin D, Liu C T, Yang Z B, Yip S and Ho J C 2023 *Adv. Mater.* **35** 2210854
[57] Zhang W, Zhang L, Wong P K J, Yuan J, Vinai G, Torelli P, Van Der Laan G, Feng Y P and Wee A T S 2019 *ACS Nano* **13** 8997
[58] Zhang B H, Hou Y S, Wang Z and Wu R Q 2021 *Phys. Rev. B* **103** 054417
[59] Miwa S, Suzuki M, Tsujikawa M, Matsuda K, Nozaki T, Tanaka K, Tsukahara T, Nawaoka K, Goto M, Kotani Y, Ohkubo T, Bonell F, Tamura E, Hono K, Nakamura T, Shirai M, Yuasa S and Suzuki Y 2017 *Nat. Commun.* **8** 15848
[60] Kresse G and Hafner J 1993 *Phys. Rev. B* **47** 558
[61] Kresse G and Furthmüller J 1996 *Phys. Rev. B* **54** 11169
[62] Kresse G and Furthmüller J 1996 *Comput. Mater. Sci.* **6** 15
[63] Perdew J P, Burke K and Ernzerhof M 1996 *Phys. Rev. Lett.* **77** 3865
[64] Blöchl P E 1994 *Phys. Rev. B* **50** 17953
[65] Grimme S, Antony J, Ehrlich S and Krieg H 2010 *J. Chem. Phys.* **132** 154104
[66] Li J Q, Cheng C and Duan M Y 2023 *Appl. Surf. Sci.* **618** 156541
[67] Yu J B and Sun Q 2018 *Appl. Phys. Lett.* **112** 053901
[68] Yang H X, Liang J H and Cui Q R 2023 *Nat. Rev. Phys.* **5** 43
[69] Boulle O, Vogel J, Yang H X, Pizzini S, Chaves D de S, Locatelli A, Klein O, Belmeguenai M, Roussigné Y, Stashkevich A, Chérif S M, Aballe L, Foerster M, Chshiev M, Auffret S, Miron I M and Gaudin G 2016 *Nat. Nanotechnol.* **11** 449
[70] Dupé B, Hoffmann M, Paillard C and Heinze S 2014 *Nat. Commun.* **5** 4030
[71] Cui Q R, Zhu Y M, Ga Y L, Liang J H, Li P, Yu D X, Cui P and Yang H X 2022 *Nano Lett.* **22** 2334
[72] Rohart S and Thiaville A 2013 *Phys. Rev. B* **88** 184422
[73] Jia H Y, Zimmermann B and Blügel S 2018 *Phys. Rev. B* **98** 144427
[74] Muckel F, Von Malottki S, Holl C, Pestka B, Pratzer M, Bessarab P F, Heinze S and Morgenstern M 2021 *Nat. Phys.* **17** 395
[75] Müller G P, Hoffmann M, Dißelkamp C, Schürhoff D, Mavros S, Sallermann M, Kiselev N S, Jónsson H and Blügel S 2019 *Phys. Rev. B* **99** 224414
[76] Lin S Z, Saxena A and Batista C D 2015 *Phys. Rev. B* **91** 224407
[77] Cui Q R, Zhu Y M, Jiang J W, Liang J H, Yu D X, Cui P and Yang H X 2021 *Phys. Rev. Res.* **3** 043011
[78] Jiang J W, Liu X, Li R and Mi W B 2021 *Appl. Phys. Lett.* **119** 072401
[79] Li P, Cui Q R, Ga Y L, Liang J H and Yang H X 2022 *Phys. Rev. B* **106** 024419
[80] Hervé M, Dupé B, Lopes R, Böttcher M, Martins M D, Balashov T, Gerhard L, Sinova J and Wulfhekel W 2018 *Nat. Commun.* **9** 1015
[81] Mühlbauer S, Binz B, Jonietz F, Pfleiderer C, Rosch A, Neubauer A, Georgii R and Böni P 2009 *Science* **323** 915
[82] Chen S H, Lourembam J, Ho P, Toh A K J, Huang J F, Chen X Y, Tan H K, Yap S L K, Lim R J J, Tan H R, Suraj T S, Sim M I, Toh Y T, Lim I, Lim N C B, Zhou J, Chung H J, Lim S T and Soumyanarayanan A 2024 *Nature* **627** 522
[83] Seki S, Yu X Z, Ishiwata S and Tokura Y 2012 *Science* **336** 198
[84] Moreau-Luchaire C, Moutafis C, Reyren N, Sampaio J, Vaz C A F, Van Horne N, Bouzehouane K, Garcia K, Deranlot C, Warnicke P, Wohlhüter P, George J-M, Weigand M, Raabe J, Cros V and Fert A 2016 *Nat. Nanotechnol.* **11** 444
[85] Du W, Dou K, He Z, Dai Y, Huang B and Ma Y 2022 *Nano Lett.* **22** 3440